H_2CO AND OH LINE OBSERVATIONS OF THE CHAMAELEON I DARK CLOUD

M. Toriseva[1], B. Höglund[2], K. Mattila[1]

RESUMEN. Se presenta el primer mapa extenso de la nube oscura Camaleón I, en radio-frecuencias correspondientes a líneas. Se usó el radiotelescopio de 64 m de Parkes para obtener mapas en la línea de 6 cm de la absorción de formaldehído, y en la línea de 18 cm de la emisión de OH. El espaciado de la grilla fue de 6' en H_2CO y de 10' en OH, prácticamente el diámetro del haz del telescopio en las respectivas frecuencias. Se obtuvieron 32 puntos observados en OH y 83 en H_2CO.

Se encontró que el máximo de la línea integrada de H_2CO, 0,85 K km/s, se halla cerca de la posición $\alpha = 11^h06^m$, $\delta = -77°05'$. En OH el máximo, 1,5 K km/s, se halla unos 5' al sur del máximo en H_2CO.

La extensión de la distribución de formaldehído corresponde bien a la distribución de la extinción obtenida mediante recuentos de estrellas usando placas Schmidt, mientras que la distribución de OH es algo más amplia.

Hay tres nebulosas de reflexión asociadas con la nube, dos de ellas iluminadas por estrellas de clase B. No observamos correlación (ni anticorrelación) entre ellas y los parámetros de la línea H_2CO.

ABSTRACT. The first extensive radio line mapping of the Chamaeleon I dark cloud is reported. The Parkes 64-m radio telescope was used to map the 6-cm formaldehyde absorption and the 18-cm OH emission, with grid spacings of 6' and 10'. respectively, roughly equal to the beamwidth of the telescope at the respective frequencies. The OH observations were secured in 32 positions and the H_2CO observations in 83. The maximum integrated H_2CO line area, about 0.85 K km/s, was found near the position $\alpha = 11^h06^m$, $\delta = -77°05'$. In OH, the maximum line area, 1.5 K km/s, was some 5' S of the H_2CO peak. The extension of the H_2CO distribution corresponds well to the extinction distribution found by star counts on Schmidt plates, whereas the OH distribution is somewhat broader. There are three reflection nebulae associated with the cloud, two of them with B-type illuminating stars. There is no correlation (or anticorrelation) of the H_2CO line parameters with these nebulae.

I. INTRODUCTION

The Chamaeleon I dark cloud is a large cloud at high galactic latitude ($l = 297°$, $b = -16°$) near the star ε Chamaeleontis (Hoffmeister 1962). It is one of the few nearby dark clouds suitable for detailed study in view of the problem of low mass star formation. It has been the subject of several studies in the optical and infrared (e.g. Aitken and Roche 1981, Appenzeller 1979, Glass 1979, Grasdalen *et al.* 1975, Henize and Mendoza 1973), but radio studies have been scanty. The optical investigations have revealed a large number of young and variable

[1] Observatory and Astrophysics Laboratory, University of Helsinki, Finland.
[2] Onsala Space Observatory, Sweden.

stars, 45 stars with Hα emission, and four Herbig-Haro objects (Schwartz 1977, Schwartz and Dopita 1980). Ground-based infrared observations have revealed highly reddened stars within the cloud (Hyland *et al.* 1982), and the IRAS satellite has found a number of embedded protostars (Schorn 1984).

Star counts have been carried out in the cloud, using visual (Rydgren 1980, 1982) and blue Schmidt plates (Toriseva and Mattila 1983). The cloud mass obtained in this way by Rydgren (1980) is about 670 solar masses, assuming a distance of 140 pc. The Schmidt plates show that the cloud is in a region of extensive thin dust, this dust being indicated by the extinction, as well as by the reflection it causes. It seems to be part of a dust layer parallel to the galactic disk and some 50-70 pc south of it (King *et al.* 1980).

The reddening law in the cloud has been a subject of controversy (Glass 1979, Hyland 1980). Values of $R = A_V/E_{B-V}$ between 3 (Hyland *et al.* 1982) and 5.5 (Grasdalen *et al.* 1975, Rydgren 1980) have been quoted. A recent study (Rydgren and Vrba 1983) seems to clarify the problem with the result that the reddening law is variable within the cloud.

The 6-cm formaldehyde line was detected at 14 positions in the cloud by Goss *et al.* (1980). Their data were not extensive enough to produce a map, but they were able to determine the excitation temperature and optical depth at two positions. In the northen part of the cloud they found evidence of two velocity components. Arnal (1983) has observed the cloud in the 21-cm HI line. He detected a blended HI self-absorption component coincident with the H_2CO velocity.

II. OBSERVATIONS

The area to be observed was delineated on the basis of inspection of optical extinction on the SRC Sky Survey IIIa-J plate, field No. 38. The dark cloud complex observed comprises the clouds 132-135 in Sandqvist's (1977) catalog. According to Sandqvist, the clouds are of opacity class 5 on Lynds' (1962) 1 to 6 scale. Along increasing right ascension, clouds 132 and 133 are the two small cloudlets in the western part of the field (see Fig. 2). Cloud 134 is the northern tip of the large elongated complex, and cloud 135 is the bulk part of this complex.

Our observations were made with the Parkes 64-m radio telescope in April and September, 1979 (H_2CO) and in June, 1979 (OH). The 1024-channel autocorrelator was used. During the observations, it was split into two 512-channel units, whose spectra were later averaged. The same signal from the receiver was fed to both halves of the autocorrelator. There is a difference between the phasing of the sampling in the two halves. Thus, by averaging the two units, a reduction in RMS noise is achieved (Gardner 1980). Frequency switching within the band was used in such a way that the line was observed during both the signal and the reference phase. After folding, the final 256-channel spectra were obtained. Hanning smoothing was applied to all spectra. The observational parameters are shown in Table 1.

TABLE 1

PARAMETERS OF THE OBSERVATIONS

	H_2CO	OH
Bandwidth	500 kHz	200 kHz
Resolution	0.12 km/s	0.14 km/s
System temperature	48-65 K	80-110 K
Beamwidth	4.4 arcmin.	12 arcmin.
Grid spacing	6 arcmin.	10 arcmin.
N. of obs. points	83	32

The antenna pointing accuracy was about 15". The antenna temperature scale was checked using the formaldehyde absorption line in NGC 2024. The observed values had to be corrected by a factor of 1.22 (April) or 0.89 (September) to obtain the antenna temperature of T_A= 4.6 K for this source, as given by Goss *et al.* (1980). The assumed beam efficiency is 65 %.

In OH, a beam efficiency of 70 % was adopted (Vaile and Taylor, 1982). The absorption lines of RCW 36 were observed for calibration at 1667 MHz (Manchester *et al.* 1970), and the absorption line of 333.6-0.2 at 1612 MHz (Goss *et al.* 1970). The calibration at 1612 and 1667 MHz was correct to within 10%. We assume that the 1667 MHz calibration is valid for 1665 MHz as

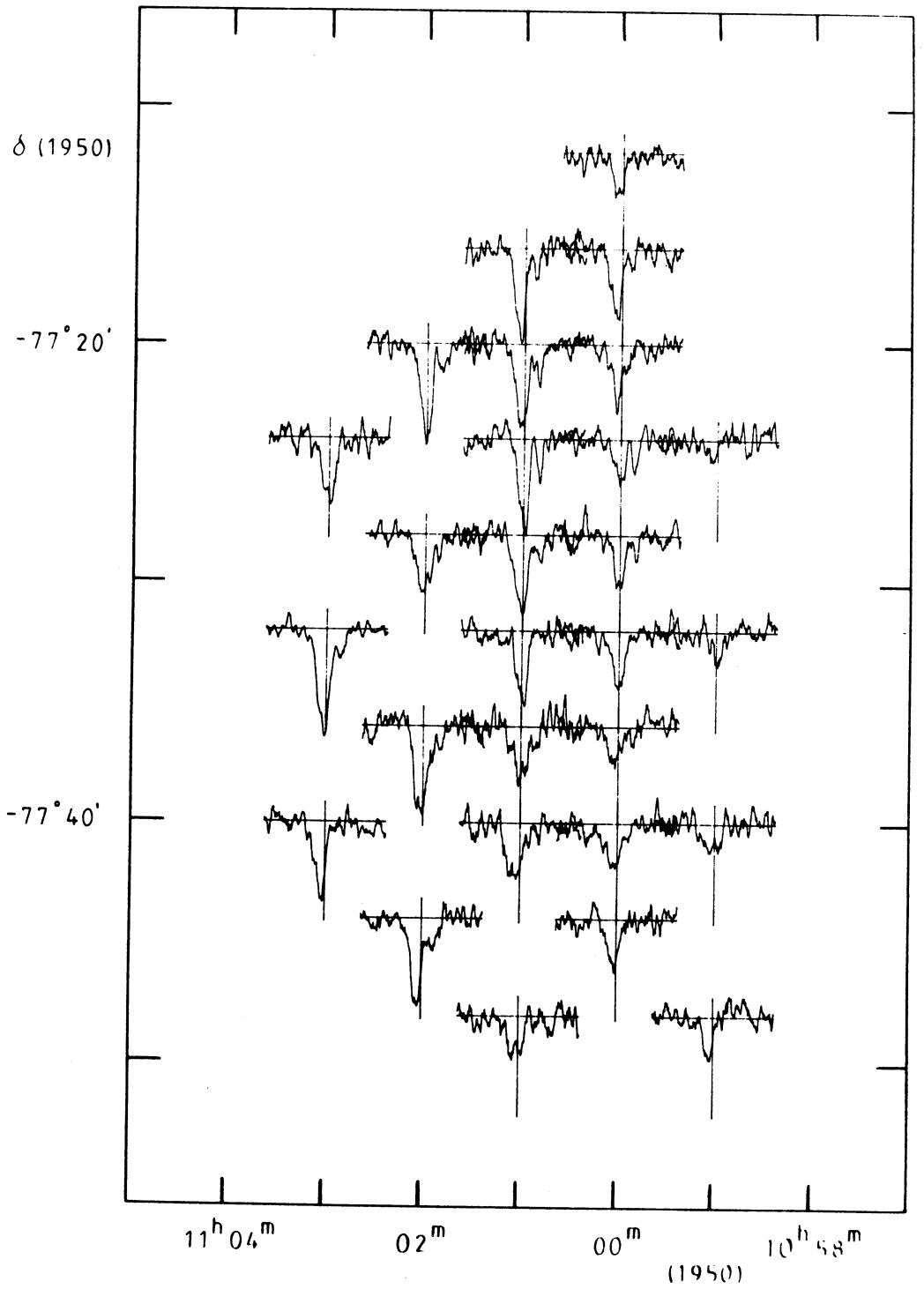

Fig. 1. A sample of the observations for the H_2CO map. The spectra in the SW part of the Cha I cloud, smoothed over 5 channels, are plotted. This is the part where 4' grid spacing was used (elsewhere 6').

well, and that our 1720 MHz data are reliable, even though calibrated by noise tube only.

III. RESULTS

1. The H_2CO map

We mapped the cloud in the 6-cm formaldehyde line with a grid spacing of 6' over most of the cloud, and with 4' in the SW part in order to look for smaller-size structures. In Fig. 1 we show the H_2CO spectra in this region, smoothed over 5 channels. No abrupt variations are seen. Fig. 2 shows the integrated line area contour map superimposed on the SRC blue Sky

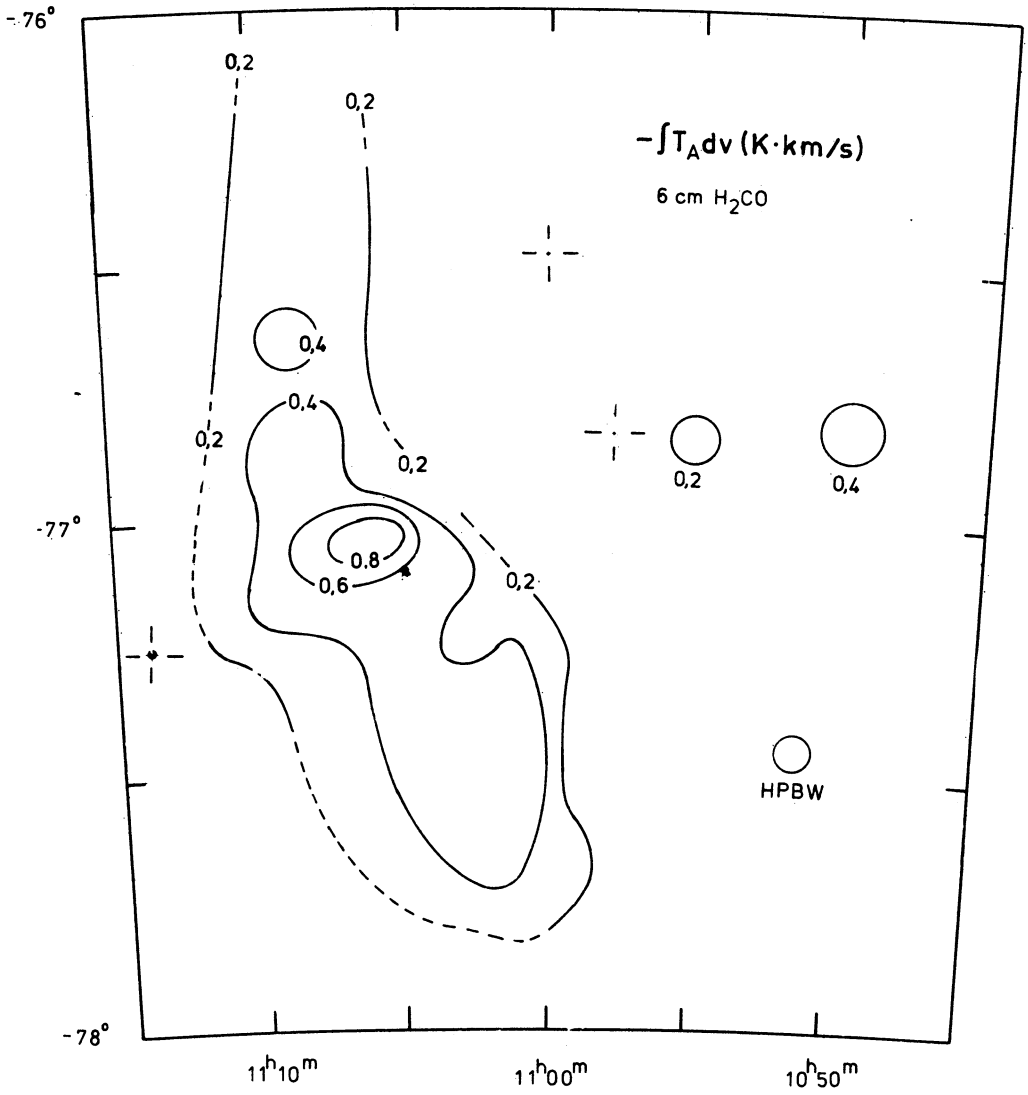

Fig. 2. Integrated H_2CO line area contour map, superimposed on the SRC blue Sky Survey plate. The coordinates are for 1950.0.

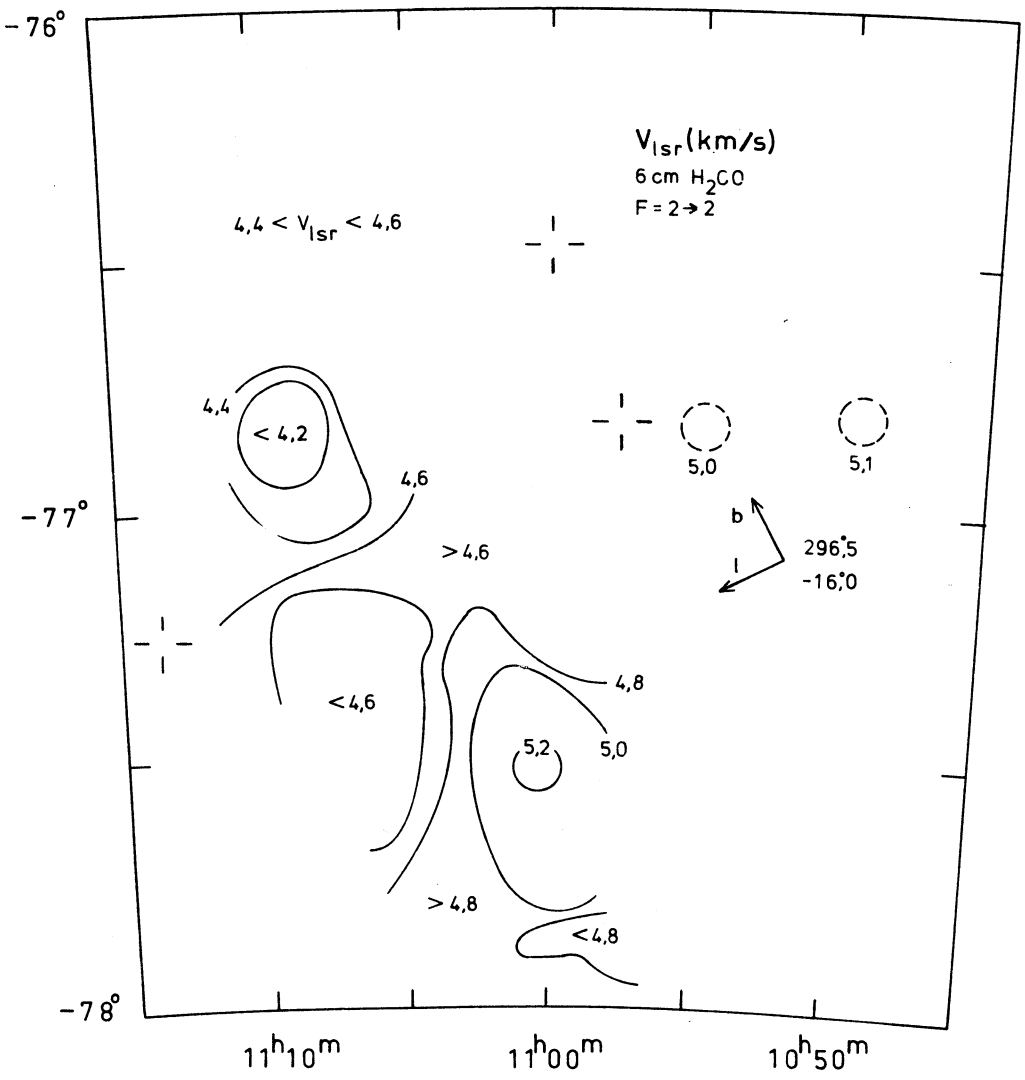

Fig. 3. The isovelocity contours of the H_2CO line. The velocity is for the 2-2 hyperfine transition of the 6-cm line. The position of the cloud with respect to galactic coordinates is indicated. The equatorial coordinates are for 1950.0.

Survey plate. Fig. 3 shows the isovelocity contours and Fig. 4 the linewidth, each for the single hyperfine transition 2-2. Fig. 5 shows the distribution of the peak antenna temperature, obtained by fitting a Gaussian to the blended line. This line includes the five nearby hyperfine components (the 1-0 satellite component is excluded). Our formaldehyde results are in good agreement with those of Goss *et al.* (1980).

In the vicinity of the direction $\alpha = 11^h01^m$, $\delta = -77°23'$, we see a substantial apparent enhancement of the 1-0 satellite transition. This implies high optical depth, since the

alternative explanations lack credibility: different excitation temperatures for the 2-2 and 1-0 hyperfine transitions are not known to exist, and another velocity component, accidentally occurring exactly at the velocity which corresponds to the 1-0 line, would, in addition, have to follow the velocity gradient of the main component in this region (see Fig. 1). Goss *et al.* (1980) discovered a secondary velocity component at the northern end of the cloud complex (i.e., at Sandqvist's cloud 134) at a velocity of 5.2 km/s.

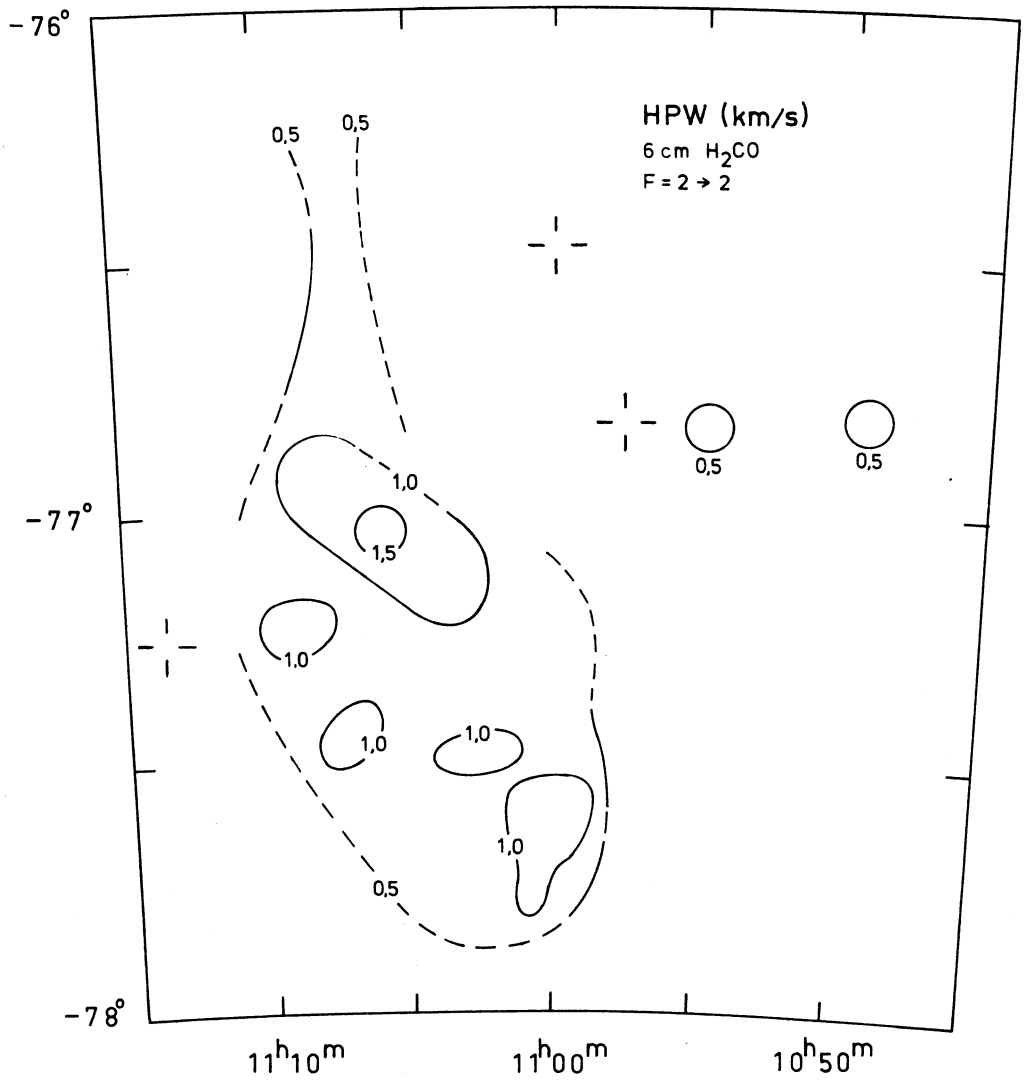

Fig. 4. The half-power linewidth of the 2-2 transition of the 6-cm line. The coordinates are for 1950.0.

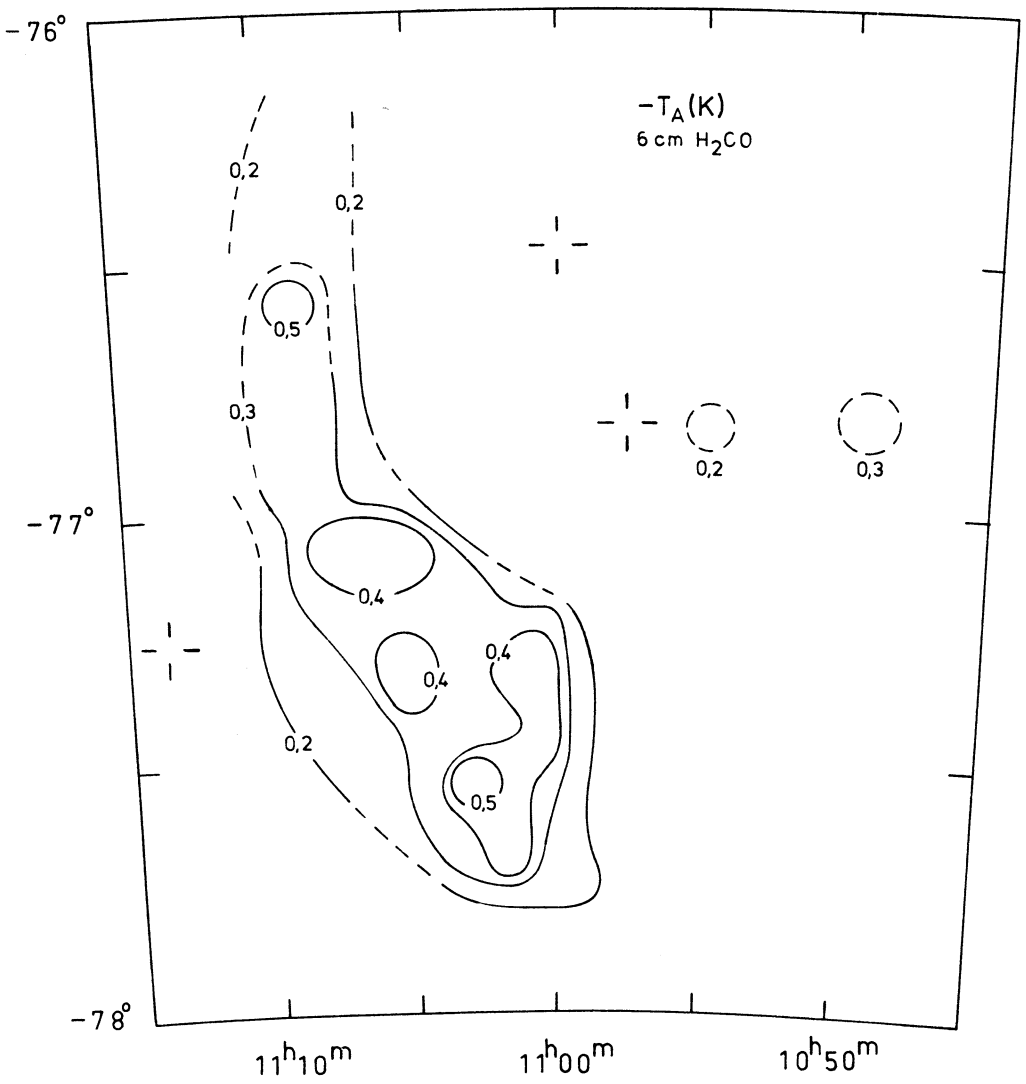

Fig. 5. The antenna temperature map in the 6-cm H_2CO line (it corresponds to the peak of the envelope of the hyperfine blend). The coordinates are for 1950.0.

In Fig. 6 we see the average of the H_2CO spectra in the positions $\alpha = 11^h01^m$, $\delta = -77°20'$ and $\alpha = 11^h01^m$, $\delta = -77°24'$, shifted in frequency with respect to one another in order to compensate for the velocity gradient. In the Gaussian fit calculation, a large value (say $\tau > 5$) of the optical depth of the 2-2 transition was necessary for a good fit. The fitted curve superimposed on the spectrum in Fig. 6 was calculated using $\tau = 10$.

The signal-to-noise ratio was insufficient for the determination of the excitation temperature and optical depth at individual positions. Even by adding several adjacent observations, we were unable to determine those parameters. If we allow for T_{ex} values between 1 and 2K, then the optical depth in the southern part of the cloud is between 0.2 and 0.6, respectively. From the work of Goss *et al.* (1980), we adopted the value of 1.4 K for our calculations, and assume that it is the same over the whole cloud.

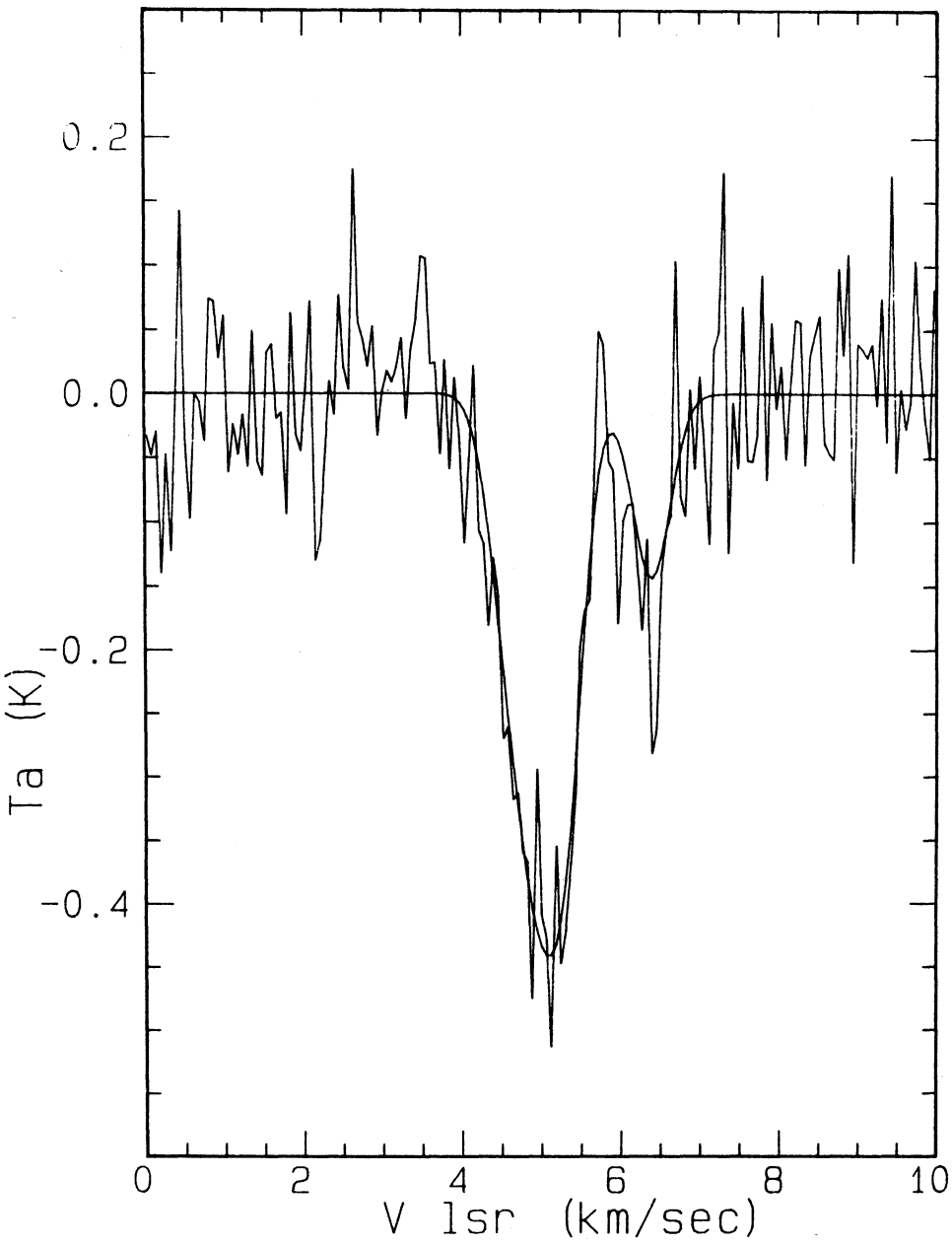

Fig. 6. The average of the H_2CO spectra at the positions $\alpha = 11^h01^m$, $\delta = -77°20'$ and $\alpha = 11^h01^m$, $\delta = -77°24'$, shifted in frequency with respect to one another to compensate for the velocity gradient. The parameters for the Gaussian fit curve were calculated using optical depth $\tau = 10$.

We calculated the formaldehyde column density from the approximate relationship (e. g. Poppel *et al.* 1983)

$$N_1 = 1.45 \times 10^{13} \frac{T_{ex}}{\eta_B (T_{ex} - T_{bg})} \int T_A(v)\, dv \quad ,$$

where η_B is the beam efficiency (65 %), T_{ex} is the excitation temperature, and $\int T_A(v)dv$ is the integrated line area (in K km/s). This is the column density of orthoformaldehyde in the 1_{11} state (the lower state of the 6-cm transition), in units of cm^{-2}. The complex problem of obtaining the total column density of formaldehyde has been treated by Javanaud (1979), among others. Assuming a normal ortho-para ratio and normal occupation numbers of the higher energy levels, an approximate total column density is obtained from (Scoville *et al.* 1972).

$$N(H_2CO) = 3 \times N_1 \ cm^{-2}.$$

It is easy to see that the column density N_1 depends critically on the excitation temperature. The column density map has the same appearance as the integrated line intensity map (Fig. 2), with the scaling

$$N_1 = - 2.4 \times 10^{13} \int T_A(v)dv \ cm^{-2} \ .$$

Over most of the cloud, the column density N_1 is within $(1.0\pm0.5)\times10^{13}$ cm^{-2}. This result is quite normal in comparison to the values obtained for other clouds. For the Taurus cloud, Heiles and Gordon (1975) obtained column densities within the range $0.5\text{-}5\times10^{13}$ cm^{-2}. The same range was obtained by Sandqvist and Lindroos (1976) for a group of southern dark clouds. For the ρ Oph cloud, Myers and Ho (1975) obtained the column density $N_1 = 3.2\times10^{13}$ cm^{-2}.

2. The OH map

The antenna temperature map of the 1667 MHz OH line is shown in Fig. 7. The line parameters (integrated area, velocity, linewidth, and peak antenna temperature) are given in Table 2 in the form of a numerical map. This line is stronger than what is usually observed in dark clouds. To our knowledge, the 1667 MHz OH line antenna temperature at its maximum, T_A = 1.3 K, is higher than in any other dark cloud. The OH molecule is found in a much larger area than H_2CO, and in fact our observations fail to indicate the limit of the OH distribution.

TABLE 2

NUMERICAL MAP OF THE CHAMAELEON I CLOUD IN THE 1667 MHz LINE*

Declination (1950)					
		0.30			
-76°20'		4.48			
		0.62			
		0.54			
		0.57			Integrated Line Area
32'		4.54			Radial Velocity
		0.62			Half-Power Linewidth
		0.84			Antenna Temperature
	0.36	0.80			
44'	4.37	4.33			
	1.20	1.09			
	0.29	0.71			
56'	0.77	1.03	1.10		
	4.45	4.29	4.64		
	1.71	1.32	1.85		
	0.41	0.73	0.56		
		1.33		0.92	
-77°02'		4.45		4.74	
		1.26		1.25	
		1.03		0.74	

TABLE 2 (continued)

	0.98	1.29	1.47	0.88	
08'	4.51	4.54	4.59	4.60	
	0.94	0.89	1.16	1.35	
	0.94	1.34	1.14	0.64	
	1.03	1.17	1.47		
14'	4.48	4.51	4.68		
	0.92	0.91	1.11		
	1.03	1.19	1.26		
	0.68	0.89	1.27	1.18	0.80
20'	4.42	4.56	4.66	4.83	4.80
	1.12	0.92	1.08	1.10	0.98
	0.59	0.89	1.13	1.05	0.78
		0.87	1.02		
26'		4.53	4.82		
		1.10	0.98		
		0.75	1.04		
		0.74	0.85	1.11	0.84
32'		4.54	4.62	4.84	4.95
		1.30	0.88	1.15	0.89
		0.56	0.90	0.91	0.75
44'			0.42	1.02	0.94
			4.63	4.78	4.87
			0.89	0.89	1.18
			0.51	0.91	0.79
Right Ascension (1950)					
11^h12^m		09^m	06^m	03^m	00^m

* The quantities from top to bottom are: integrated line area (K km/s); radial velocity (km/s); half-power linewidth (km/s); and peak antenna temperature (K). Their average standard deviations are 0.09, 0.08, 0.07, and 0.05, respectively.

At five positions, we observed other lines in addition to the 1667 MHz line, and all the four lines were observed at one of these positions. The line parameters at these five positions, as obtained from Gaussian fitting, are given in Table 3. The errors are 1 σ.

The main line peak antenna temperatures are plotted in Fig. 8. The two upper straight lines are the predicted relationships for LTE, i.e. when the excitation temperatures of the two transitions are equal. The assumed optical depths of the 1667 MHz transition are indicated. The lowest line is a nearest-fit line drawn by eye. It is seen that our results indicate deviations from the local thermodynamical equilibrium in the main lines as well as in the satellite lines (Table 2). However, the statistical significance of this result is not fully convincing, since we did not have a separate intensity scale calibration at 1665 MHz, but had to use the calibration at 1667 MHz (i.e., the absorption line of RCW 36) also for 1665 MHz. We find that the 1612 and 1665 MHz lines are weaker relative to 1667 MHz than what is compatible with the LTE ratios 1:5:9:1. The 1720 MHz lines is correspondingly stronger, if the calibration is correct. The 1612 MHz line was below our detection limit. Apart from the main line anomaly, these results are in qualitative agreement with the OH excitation theory of Guibert *et al.* (1978).

We calculated the OH column density from (see, e.g., Mattila *et al.* 1979)

$$N(OH) = 4.03 \times 10^{13} \frac{T_{ex}}{\eta_B (T_{ex} - T_{bg})} \int T_A(\nu)\, d\nu \quad ,$$

where the line area is in units of K kHz. This relationship, which depends mainly on the integrated line area, is suitable for our case, where it was impossible to determine the excitation temperature T_{ex} or the optical depth for the 1667 MHz line. The equation is valid for a small optical depth. The use of this equation is justified by our data (Fig. 8), and by Crutcher's (1979) analysis.

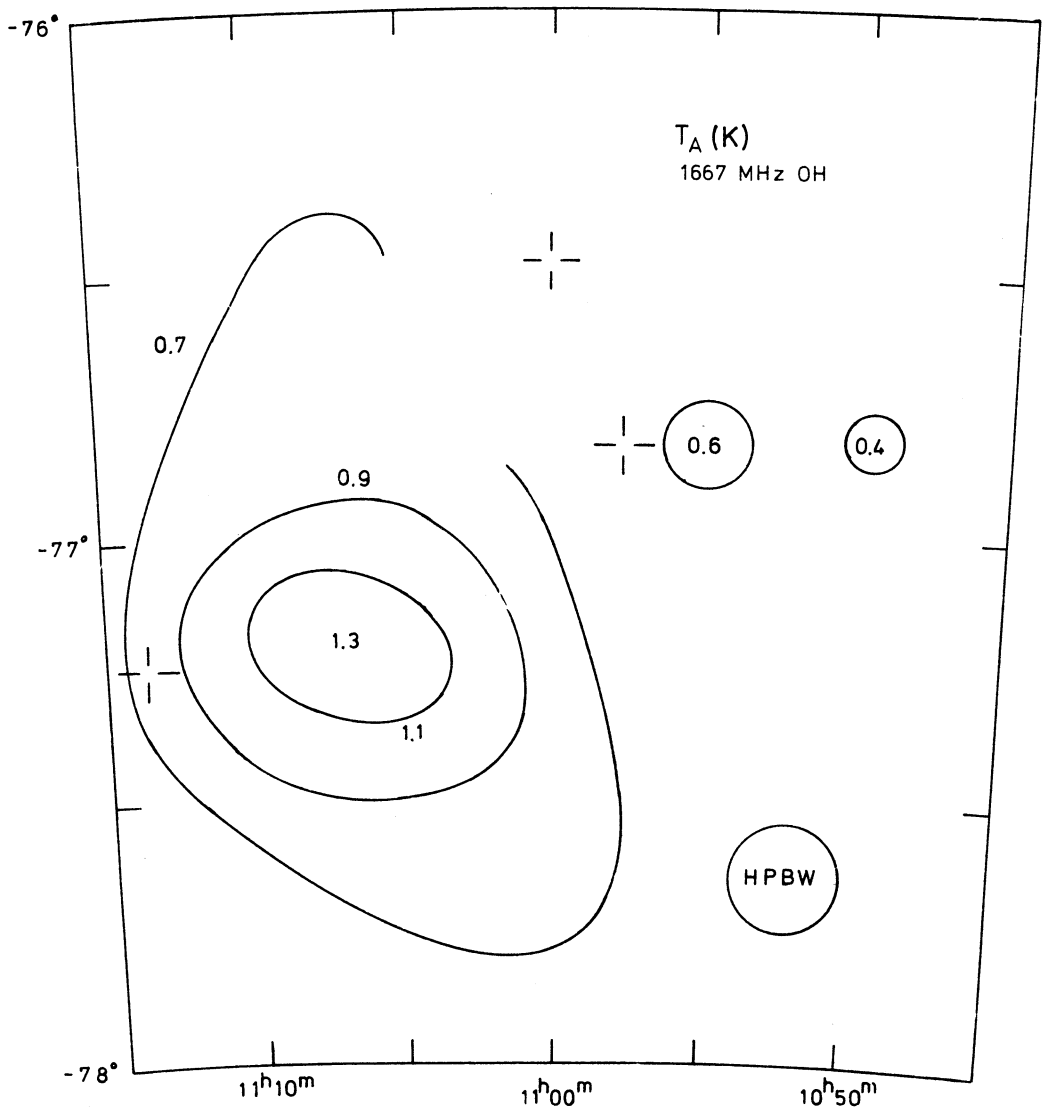

Fig. 7. Peak antenna temperature of the 1667 MHz OH line. The coordinates are for 1950.0.

If we assume the rather normal values T_{ex} = 6 K and T_{bg} = 2.7 K for the excitation and the background brightness temperatures, respectively, we obtain N(OH) values within the range (1.56 to 7.63)x10^{14} cm^{-2} all over the observed area. If we allow the T_{ex} variation to be between 4.5 and 17 K (the normal range of values observed in dark clouds), the error in N(OH) remains within 35 %.

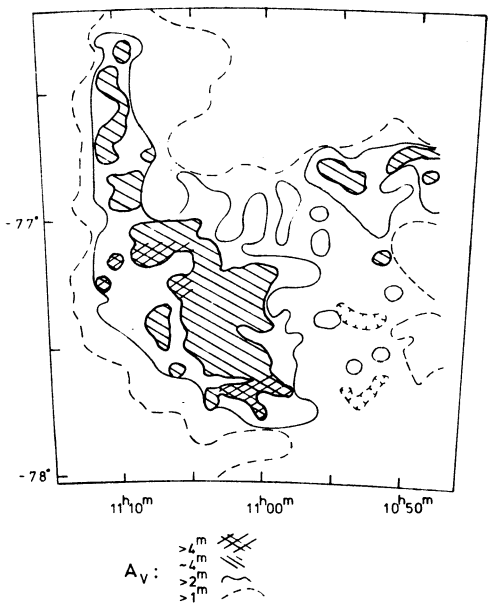

Fig. 8. Relationship of the antenna temperatures for the 1665 and 1667 MHz OH lines. The 1667/1665 MHz line ratio is anomalously high. The two upper straight lines are the predicted relationships, assuming LTE and the 1667 MHz optical depth values indicated. The lowest line is nearest-fit line drawn by eye.

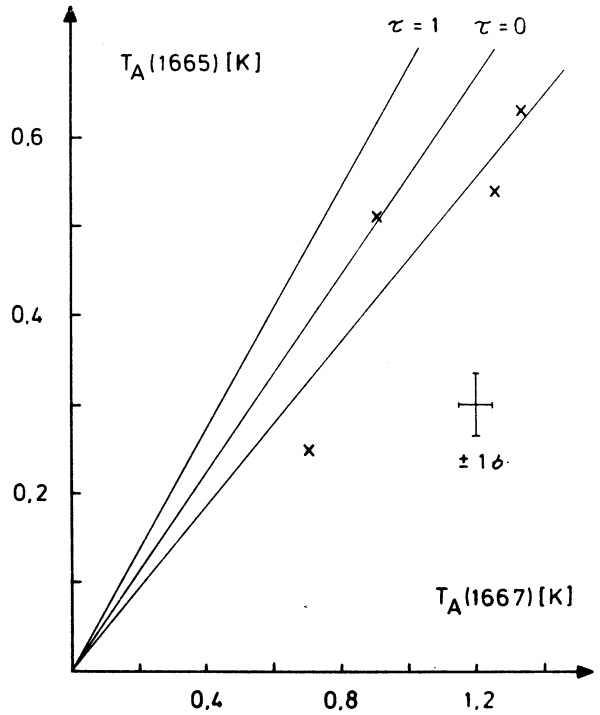

Fig. 9. Visual extinction map, based on Rydgren's (1980) star counts.

The corresponding peak values of the integrated line are 0.85 K km/s and 1.5 K km/s, respectively.

The correlation between H_2CO and OH antenna temperatures is weak (Fig. 10). The equations of the two regression lines are:

TABLE 3

ANTENNA TEMPERATURES IN THE POINTS WHERE OTHER OH TRANSITIONS IN ADDITION TO 1667 MHz WERE OBSERVED*

Freqs. in MHz		1612	1665	1667	1720
Position (1950)					
$11^h\ 3^m$	-77° 32'		0.51 ±0.04	0.91 ±0.05	
$11^h\ 4^m\ 30^s$	-77° 14'		0.54 ±0.04	1.26 ±0.04	
$11^h\ 6^m$	-77° 20'			1.13 ±0.05	(0.26) ±0.04
$11^h\ 9^m$	-76° 44'		0.25 ±0.03	0.71 ±0.05	
$11^h\ 9^m$	-77° 08'	0.04 ±0.02	0.63 ±0.03	1.34 ±0.05	(0.28) ±0.06

* 1720 MHz calibration by noise tube only. The errors are 1 σ.

Adopting $A_V = 5^m$ (which may be an underestimate) at the OH peak position, we have $N(OH)/A_V = 1.5 \times 10^{13}$ cm^{-2}mag^{-1}, which is higher, by a factor of about two, than the average value obtained by Crutcher (1979) in his analysis of several dark clouds.

3. Extinction map

Star count data from a visual Cerro Tololo Curtis Schmidt plate was kindly provided by Dr. A.E. Rydgren (1980, 1982). Based on these counts we have drawn the visual extinction map which is shown in Fig. 9. It is seen that the visual extinction is 4^m or more over large areas of the cloud, and there are three areas where it may be considerably higher. These extinction values are based on a cumulative star number function with the gradient $\frac{\log\Delta N(m)}{\Delta m} = 0.35$, which is probably too high (Toriseva and Mattila 1983) and leads to underestimated extinctions. Based on infrared observations of background stars, Hyland *et al.* (1982) have derived the extinction in the northern part of the cloud. They obtained E(J-K) values in the direction of 41 background stars in the region $\alpha = 11^h07^m$ to 11^h12^m, $\delta = -76°15'$ to $-76°50'$. Assuming $A_V = 6.25 \times E(J-K)$, they obtained $A_V = 7^m$ along a N-S ridge at about 11^h09^m. However, Rydgren's visual star count map gives only $A_V = 4^m$ along this ridge.

IV. DISCUSSION

1. Comparison of formaldehyde and OH

A substantial difference is observed between the formaldehyde and OH antenna temperature maps (Figs. 5 and 7). In H_2CO, we see (Fig. 5) four or five roughly equal maxima within the large elongated cloud complex, which would remain even if we smoothed the H_2CO map to the OH beamsize. The OH molecule (Fig. 7) extends farther to the east than H_2CO, and the general appearance of the OH map is much rounder than that of the elongated H_2CO map, even if we allow for the influence of the large beamsize.

We cannot say conclusively whether this difference between OH and H_2CO is due to a more rapid decrease of the H_2CO column density with decreasing extinction, or whether it is due to the lack of sufficient pumping for the H_2CO anomalous absorption to be observable.

The peak of the H_2CO column density is near the position (Fig. 2) $\alpha = 11^h06^m$, $\delta = -77°05'$, while the OH peak is at the same right ascencion but at about $\delta = -77°10'$ (Table 2).

$$T_A(OH) = 1.36\ |T_A(H_2CO)| + 0.46 \quad (H_2CO \rightarrow OH)$$

and

$$T_A(OH) = 5.14\ |T_A(H_2CO)| - 0.70 \quad (OH \rightarrow H_2CO)$$

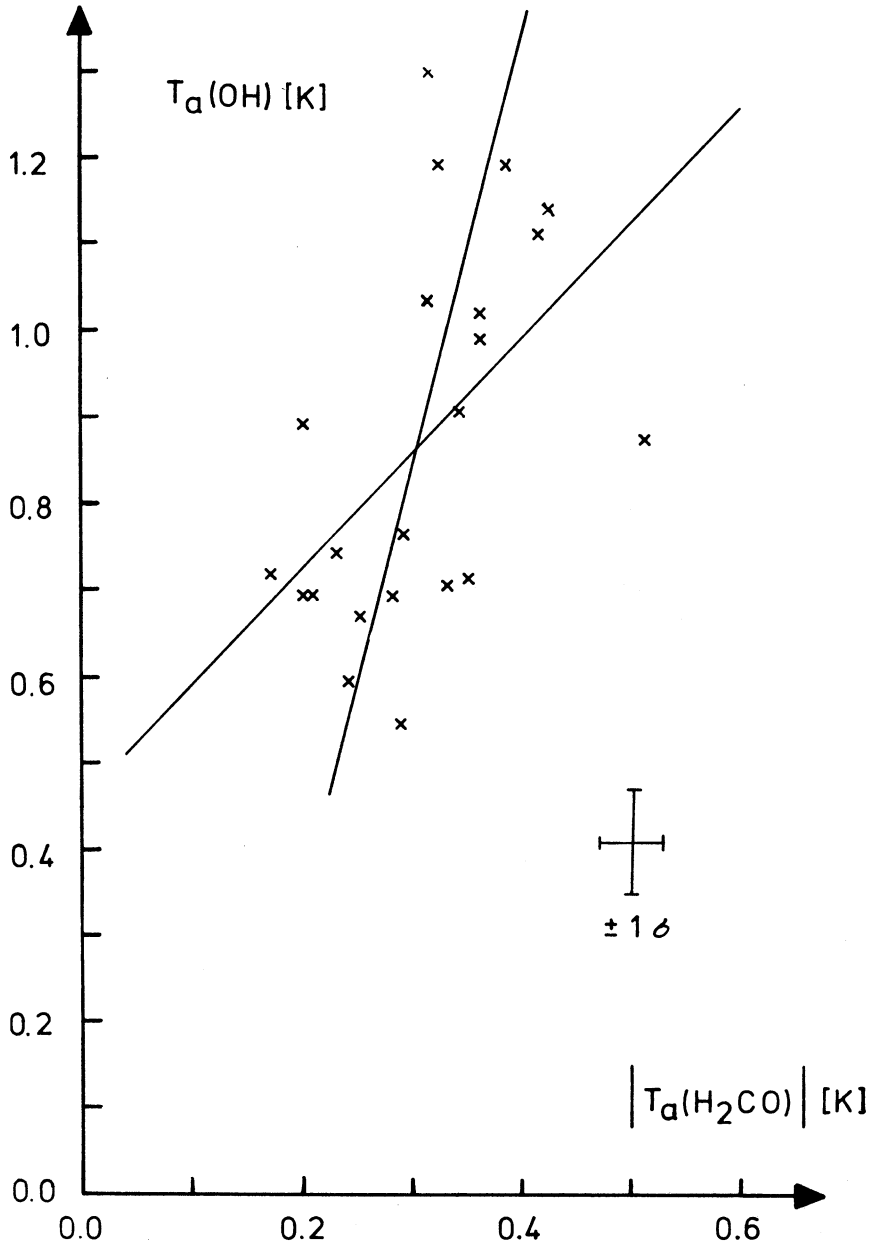

Fig. 10. Comparison of OH (1667 MHz) and H_2CO antenna temperatures.

The correlation coefficient is 0.51, which is quite normal in comparison to coefficients published in the literature. In our case the correlation is impaired by 1:3 ratio in the beamsizes and by the sparser grid of observations in OH than in H_2CO (Table 1). The comparison was made

between original OH antenna temperatures and interpolated H_2CO antenna temperatures. For the Taurus dark cloud, which is largely similar to the Chamaeleon cloud, Turner and Heiles (1974) obtained correlation coefficients of 0.44 and 0.67. For the small L134 cloud, which has an opaque core, Mattila *et al.* (1979) obtained the high correlation coefficient of 0.78.

2. Comparison of formaldehyde with extinction and effects of bright stars

The integrated formaldehyde line intensity agrees quite well with the optical extinction map, based on star counts by Rydgren (1980, 1982) on a visual Cerro Tololo Curtis Schmidt plate (Fig. 9).

We wanted to look for a possible correlation between H_2CO column density and the bright stars associated with the cloud. The sensitivity of formaldehyde to dissociation by UV radiation is well known (e.g. Sandell and Mattila 1975, Bernes and Sandqvist 1977). In the ρ Oph cloud, Myers and Ho (1975) found a possible deficiency of formaldehyde in the direction of a reflection nebula, which is illuminated by an early B-type star. There are three conspicuous reflection nebulae in the Chamaeleon cloud (Cederblad 1946, Bernes 1977). Their coordinates and illuminating stars are given in Table 4. The illuminating stars are late B stars in two cases, and a G star in the third. Comparing the integrated line area map with the location of the reflection nebulae (see Fig. 2), we conclude that there is no obvious formaldehyde deficiency (or enhancement) associated with the nebulae.

TABLE 4

THE THREE LARGE REFLECTION NEBULAE IN THE CHAMAELEON CLOUD*

Refl. nebula	Star	Spectral class	Coord. of neb. (1950.0)
Ced 110	Anon.	G2	$11^h\ 5.0^m$ -77° 06'
Ced 111	HD 97048	B9.5Ve	$11^h\ 6.8^m$ -77° 23'
Ced 112	CoD-75°523	B9.5V	$11^h\ 8.5^m$ -76° 21'

* The coordinates are from Bernes (1977).

3. Structure and kinematics of the cloud

The cloud is elongated in the direction perpendicular to the galactic plane (Fig. 3). The average velocity of both H_2CO and OH is 4.7 km/s. The cloud is at an angular distance of about 20° from the equator of Gould's Belt at the fringes of the Lower Centaurus-Crux (LCC) subdivision of the Scorpio-Centaurus association of early type stars, and is at nearly the same distance as these stars (Lesh 1972). The velocity that corresponds to Lindblad's HI Feature A in the cloud's direction is 1-2 km/s (Lindblad *et al.* 1973), implying that the cloud may be connected to Gould's Belt. There is a clear gradient in the velocity distribution of both OH and formaldehyde, the velocity in the SW part of Sandqvist's (1977) cloud 135 being about 1 km/s higher than in the NE part. This gives the impression that the cloud is rotating around an axis which is roughly perpendicular to the axis of the Galaxy. However, the velocity pattern is far from symmetric. Since the cloud is clearly in a star-forming phase, one can speculate that the velocity pattern partly reflects contraction movements.

V. CONCLUSIONS

The maps resulting from our study provide basic information on the density distribution of molecules in the cloud, thus bringing out points of interest for further (e.g., CO) observations. More sensitive H_2CO and OH observations are needed to determine the excitation temperature and optical depth in the cloud.

This research was made possible by a grant from the Australian Department of Education, which is gratefully acknowledged by M.T. We thank Lynette M. Newton and Niklas Holsti for their help in the transfer of the data between computers in Australia and Finland. The observing time at the Parkes telescope was assigned by the CSIRO Division of Radiophysics. We thank Dr. E. M. Arnal and Dr. A.E. Rydgren for making available their unpublished results.

REFERENCES

Aikten, D.K. and Roche, P.F. 1981, *M.N.R.A.S.* 196, 39P.
Appenzeller, I. 1979, *Astr. Ap.* 71, 305.
Arnal, E.M. 1983, private communication.
Bernes, C. 1977, *Astr. Ap. Suppl.* 29, 65.
Bernes, C. and Sandqvist, Aa. 1977, *Ap. J.* 217, 71.
Cederblad, S. 1946, *Lund Meddelanden*, S. II, N° 119.
Crutcher, R.M. 1979, *Ap. J.* 234, 881.
Gardner, F. 1980, private communication.
Glass, I.S. 1979, *M.N.R.A.S.* 187, 305.
Goss, W.M., Manchester, R.N., and Robinson, B.J. 1970, *Australian J. Phys.* 23, 559.
Goss, W.M., Manchester, R.N., Brooks, J.W., Sinclair, M.W., Manefield, G.A., and Danziger, I.J. 1980, *M.N.R.A.S.* 191, 533.
Grasdalen, G., Joyce, R., Knacke, R.F., Strom, S.E., and Strom, K.M. 1975, *A. J.* 80, 117.
Guibert, J., Elitzur, M., and Nguyen-Q-Rieu. 1978, *Astr. Ap.* 66, 395.
Heiles, C. and Gordon, M.A. 1975, *Ap. J.* 199, 361.
Henize, K.G. and Mendoza, V.E.E. 1973, *Ap. J.* 180, 115.
Hoffmeister, C. 1962, *Zs. f. Astrophys.* 55, 290.
Hyland, A.R. 1980, in *Infrared Astronomy*, eds. C.G. Wynn-Williams and D.P. Cruikshank (Dordrecht: Reidel), p. 125.
Hyland, A.R., Jones, T.J., and Mitchell, R.M. 1982, *M.N.R.A.S.* 201, 1095.
Javanaud, C. 1979, *M.N.R.A.S.* 188, 203.
King, D.J., Taylor, K.N.R., and Tritton, K.P. 1979, *M.N.R.A.S.* 188, 719.
Lesh, J.R. 1972, in *Âge des Etoiles*, IAU Colloquium N° 17, eds. G. Cayrel de Strobel and A.M. Delplace, paper XXIII, p. (1-7), Meudon, Paris.
Lindblad, P.O., Grape, K., Sandqvist, Aa., and Schober, J. 1973, *Astr. Ap.* 24, 309.
Lynds, B.T. 1962, *Ap. J. Suppl.* 7, 1.
Manchester, R.N., Robinson, B.J., and Goss, W.M. 1970, *Australian J. Phys.* 23, 751.
Mattila, K., Winnberg, A., and Grasshoff, M. 1979, *Astr. Ap.* 78, 275.
Myers, P.C. and Ho, P.T.P. 1975, *Ap. J. Letters* 202, L25.
Pöppel, W.G.L., Rohlfs, K., and Celnik, M. 1983, *Astr. Ap.* 126, 152.
Rydgren, A.E. 1980, *A. J.* 85, 444.
Rydgren, A.E. 1983, private communication.
Rydgren, A.E. and Vrba, F.J. 1983, *Bull. A.A.S.* 15, 653.
Sandell, G. and Mattila, K. 1975, *Astr. Ap.* 42, 357.
Sandqvist, Aa. 1977, *Astr. Ap.* 57, 467.
Sandqvist, Aa. and Lindroos, K.P. 1976, *Astr. Ap.* 53, 179.
Schorn, R.A. 1984, *Sky & Telescope*, 67, 119.
Schwartz, R.D. 1977, *Ap. J. Suppl.* 35, 161.
Schwartz, R.D. and Dopita, M.A. 1980, *Ap. J.* 236, 543.
Scoville, N.Z., Solomon, P.M., and Thaddeus, P. 1972, *Ap. J.* 172, 335.
Toriseva, M. and Mattila, K. 1983, in preparation.
Turner, B.E. and Heiles, C.E. 1974, *Ap. J.* 194, 525.
Vaile, R.A. and Taylor, K.N.R. 1982, *Proc. Astr. Soc. Australian* 4, 443.

M. Toriseva and K. Mattila: Observatory and Astrophysics Laboratory, University of Helsinki, Tähtitorninmäki, SF-00130 Helsinki 13, Finland.
B. Höglund: Onsala Space Observatory, Goteborg, Onsala, Sweden.